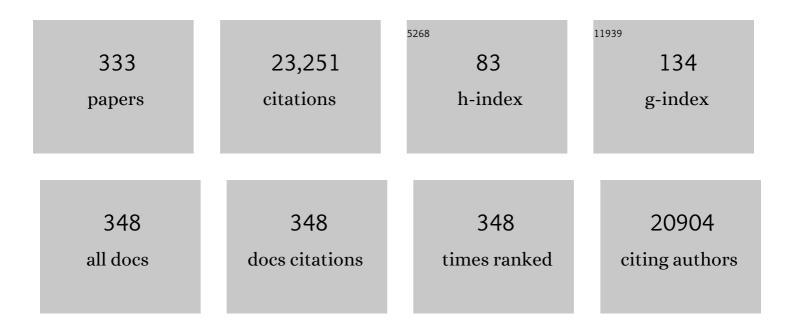
List of Publications by Year in descending order

Source: https://exaly.com/author-pdf/988404/publications.pdf Version: 2024-02-01



LASON LEVILS

#	Article	IF	CITATIONS
1	Influence of Fc Modifications and IgG Subclass on Biodistribution of Humanized Antibodies Targeting L1CAM. Journal of Nuclear Medicine, 2022, 63, 629-636.	5.0	5
2	Molecular Imaging of Neuroendocrine Prostate Cancer by Targeting Delta-Like Ligand 3. Journal of Nuclear Medicine, 2022, 63, 1401-1407.	5.0	21
3	Radioimmunotherapy Targeting Delta-like Ligand 3 in Small Cell Lung Cancer Exhibits Antitumor Efficacy with Low Toxicity. Clinical Cancer Research, 2022, 28, 1391-1401.	7.0	19
4	Noninvasive Imaging of CD4+ T Cells in Humanized Mice. Molecular Cancer Therapeutics, 2022, 21, 658-666.	4.1	3
5	EGFR-Targeted ImmunoPET of UMUC3 Orthotopic Bladder Tumors. Molecular Imaging and Biology, 2022, 24, 511-518.	2.6	5
6	ImmunoPET of Ovarian and Pancreatic Cancer with AR9.6, a Novel MUC16-Targeted Therapeutic Antibody. Clinical Cancer Research, 2022, 28, 948-959.	7.0	11
7	Caveolin-1 temporal modulation enhances antibody drug efficacy in heterogeneous gastric cancer. Nature Communications, 2022, 13, 2526.	12.8	10
8	PET Imaging of Acidic Tumor Environment With 89Zr-labeled pHLIP Probes. Frontiers in Oncology, 2022, 12, .	2.8	11
9	Pretargeted PET of Osteodestructive Lesions in Dogs. Molecular Pharmaceutics, 2022, 19, 3153-3162.	4.6	10
10	Radiotheranostics in oncology: current challenges and emerging opportunities. Nature Reviews Clinical Oncology, 2022, 19, 534-550.	27.6	92
11	Delta-like ligand 3–targeted radioimmunotherapy for neuroendocrine prostate cancer. Proceedings of the National Academy of Sciences of the United States of America, 2022, 119, .	7.1	17
12	A Systematic Evaluation of Antibody Modification and ⁸⁹ Zr-Radiolabeling for Optimized Immuno-PET. Bioconjugate Chemistry, 2021, 32, 1177-1191.	3.6	26
13	Imaging Early-Stage Metastases Using an 18F-Labeled VEGFR-1-Specific Single Chain VEGF Mutant. Molecular Imaging and Biology, 2021, 23, 340-349.	2.6	6
14	Immuno-PET Detects Changes in Multi-RTK Tumor Cell Expression Levels in Response to Targeted Kinase Inhibition. Journal of Nuclear Medicine, 2021, 62, 366-371.	5.0	4
15	Head-to-Head Evaluation of ¹⁸ F-FES and ¹⁸ F-FDG PET/CT in Metastatic Invasive Lobular Breast Cancer. Journal of Nuclear Medicine, 2021, 62, 326-331.	5.0	69
16	ImmunoPET Imaging of Pancreatic Tumors with 89Zr-Labeled Gold Nanoparticle–Antibody Conjugates. Molecular Imaging and Biology, 2021, 23, 84-94.	2.6	15
17	Antibody-Based Molecular Imaging. , 2021, , 547-562.		0
18	A simple strategy to reduce the salivary gland and kidney uptake of PSMA-targeting small molecule radiopharmaceuticals. European Journal of Nuclear Medicine and Molecular Imaging, 2021, 48, 2642-2651.	6.4	26

#	Article	IF	CITATIONS
19	Imaging Tumor-Infiltrating Lymphocytes in Brain Tumors with [64Cu]Cu-NOTA-anti-CD8 PET. Clinical Cancer Research, 2021, 27, 1958-1966.	7.0	21
20	Bimodal Imaging of Mouse Peripheral Nerves with Chlorin Tracers. Molecular Pharmaceutics, 2021, 18, 940-951.	4.6	3
21	Exploiting the MUC5AC Antigen for Noninvasive Identification of Pancreatic Cancer. Journal of Nuclear Medicine, 2021, 62, 1384-1390.	5.0	4
22	Technical Note: Patientâ€norphed meshâ€ŧype phantoms to support personalized nuclear medicine dosimetry — a proof of concept study. Medical Physics, 2021, 48, 2018-2026.	3.0	2
23	Applications of nuclear-based imaging in gene and cell therapy: Probe considerations. Molecular Therapy - Oncolytics, 2021, 20, 447-458.	4.4	13
24	REPLY TO LETTER TO THE EDITOR: POTENTIAL USE OF RADIOLABELED ANTIBODIES FOR IMAGING AND TREATMENT OF COVID-19. Journal of Nuclear Medicine, 2021, 62, jnumed.121.261950.	5.0	0
25	Synthesis and Comparative <i>In Vivo</i> Evaluation of Site-Specifically Labeled Radioimmunoconjugates for DLL3-Targeted ImmunoPET. Bioconjugate Chemistry, 2021, 32, 1255-1262.	3.6	7
26	Medical imaging and nuclear medicine: a Lancet Oncology Commission. Lancet Oncology, The, 2021, 22, e136-e172.	10.7	129
27	Recent Advances in Radiometals for Combined Imaging and Therapy in Cancer. ChemMedChem, 2021, 16, 2909-2941.	3.2	44
28	Tim-4+ cavity-resident macrophages impair anti-tumor CD8+ TÂcell immunity. Cancer Cell, 2021, 39, 973-988.e9.	16.8	93
29	State-of-the-Art of Radiometal-based Bioconjugates for Molecular Imaging and Radiotherapy. Bioconjugate Chemistry, 2021, 32, 1175-1176.	3.6	0
30	Chemical tools for epichaperome-mediated interactome dysfunctions of the central nervous system. Nature Communications, 2021, 12, 4669.	12.8	19
31	ERK Inhibition Improves Anti–PD-L1 Immune Checkpoint Blockade in Preclinical Pancreatic Ductal Adenocarcinoma. Molecular Cancer Therapeutics, 2021, 20, 2026-2034.	4.1	10
32	Imaging of Cancer γ-Secretase Activity Using an Inhibitor-Based PET Probe. Clinical Cancer Research, 2021, 27, 6145-6155.	7.0	8
33	Novel Tracers and Radionuclides in PET Imaging. Radiologic Clinics of North America, 2021, 59, 887-918.	1.8	2
34	Predicting CAR-T cell Immunotherapy Success through ImmunoPET. Clinical Cancer Research, 2021, 27, 911-912.	7.0	6
35	"Friction by Definition― Conflict at Patient Handover Between Emergency and Internal Medicine Physicians at an Academic Medical Center. Western Journal of Emergency Medicine, 2021, 22, 1227-1239.	1.1	7
36	Multimodal Positron Emission Tomography Imaging to Quantify Uptake of ⁸⁹ Zr-Labeled Liposomes in the Atherosclerotic Vessel Wall. Bioconjugate Chemistry, 2020, 31, 360-368.	3.6	22

#	Article	IF	CITATIONS
37	The Impact of Positron Range on PET Resolution, Evaluated with Phantoms and PHITS Monte Carlo Simulations for Conventional and Non-conventional Radionuclides. Molecular Imaging and Biology, 2020, 22, 73-84.	2.6	50
38	First-in-Humans Imaging with ⁸⁹ Zr-Df-IAB22M2C Anti-CD8 Minibody in Patients with Solid Malignancies: Preliminary Pharmacokinetics, Biodistribution, and Lesion Targeting. Journal of Nuclear Medicine, 2020, 61, 512-519.	5.0	170
39	An ⁸⁹ Zr-HDL PET Tracer Monitors Response to a CSF1R Inhibitor. Journal of Nuclear Medicine, 2020, 61, 433-436.	5.0	25
40	The 2019 World Molecular Imaging Congress (WMIC) and Molecular Imaging and Biology (MIB) Awards. Molecular Imaging and Biology, 2020, 22, 6-8.	2.6	0
41	Delivery of polymeric nanostars for molecular imaging and endoradiotherapy through the enhanced permeability and retention (EPR) effect. Theranostics, 2020, 10, 567-584.	10.0	63
42	Multimodality labeling strategies for the investigation of nanocrystalline cellulose biodistribution in a mouse model of breast cancer. Nuclear Medicine and Biology, 2020, 80-81, 1-12.	0.6	12
43	ImmunoPET Predicts Response to Met-targeted Radioligand Therapy in Models of Pancreatic Cancer Resistant to Met Kinase Inhibitors. Theranostics, 2020, 10, 151-165.	10.0	23
44	HER2-Targeted PET Imaging and Therapy of Hyaluronan-Masked HER2-Overexpressing Breast Cancer. Molecular Pharmaceutics, 2020, 17, 327-337.	4.6	19
45	Changing of the Guard at Molecular Imaging & Biology. Molecular Imaging and Biology, 2020, 22, 1-3.	2.6	0
46	Acute Statin Treatment Improves Antibody Accumulation in EGFR- and PSMA-Expressing Tumors. Clinical Cancer Research, 2020, 26, 6215-6229.	7.0	18
47	Antibody-Targeted Imaging of Gastric Cancer. Molecules, 2020, 25, 4621.	3.8	7
48	Comparison of Methods for Surface Modification of Barium Titanate Nanoparticles for Aqueous Dispersibility: Toward Biomedical Utilization of Perovskite Oxides. ACS Applied Materials & Interfaces, 2020, 12, 51135-51147.	8.0	15
49	Oncology-Inspired Treatment Options for COVID-19. Journal of Nuclear Medicine, 2020, 61, 1720-1723.	5.0	15
50	Polyazamacrocycle Ligands Facilitate ⁸⁹ Zr Radiochemistry and Yield ⁸⁹ Zr Complexes with Remarkable Stability. Inorganic Chemistry, 2020, 59, 17473-17487.	4.0	13
51	A High-Denticity Chelator Based on Desferrioxamine for Enhanced Coordination of Zirconium-89. Inorganic Chemistry, 2020, 59, 11715-11727.	4.0	20
52	Harnessing ⁶⁴ Cu/ ⁶⁷ Cu for a theranostic approach to pretargeted radioimmunotherapy. Proceedings of the National Academy of Sciences of the United States of America, 2020, 117, 28316-28327.	7.1	67
53	pHLIP ICG for delineation of tumors and blood flow during fluorescence-guided surgery. Scientific Reports, 2020, 10, 18356.	3.3	19
54	B7H3-Directed Intraperitoneal Radioimmunotherapy With Radioiodinated Omburtamab for Desmoplastic Small Round Cell Tumor and Other Peritoneal Tumors: Results of a Phase I Study. Journal of Clinical Oncology, 2020, 38, 4283-4291.	1.6	40

#	Article	IF	CITATIONS
55	Aromatic carbohydrate amphiphile disrupts cancer spheroids and prevents relapse. Nanoscale, 2020, 12, 19088-19092.	5.6	8
56	Leveraging synthetic chlorins for bio-imaging applications. Chemical Communications, 2020, 56, 12608-12611.	4.1	5
57	First-in-Human Trial of Epichaperome-Targeted PET in Patients with Cancer. Clinical Cancer Research, 2020, 26, 5178-5187.	7.0	18
58	Comparison of 68Ga-DOTA-JR11 PET/CT with dosimetric 177Lu-satoreotide tetraxetan (177Lu-DOTA-JR11) SPECT/CT in patients with metastatic neuroendocrine tumors undergoing peptide receptor radionuclide therapy. European Journal of Nuclear Medicine and Molecular Imaging, 2020, 47, 3047-3057.	6.4	19
59	89Zr-PET imaging of DNA double-strand breaks for the early monitoring of response following α- and β-particle radioimmunotherapy in a mouse model of pancreatic ductal adenocarcinoma. Theranostics, 2020, 10, 5802-5814.	10.0	15
60	Radiopharmacologic screening of antibodies to the unshed ectodomain of MUC16 in ovarian cancer identifies a lead candidate for clinical translation. Nuclear Medicine and Biology, 2020, 86-87, 9-19.	0.6	5
61	Identification of HER2-Positive Metastases in Patients with HER2-Negative Primary Breast Cancer by Using HER2-targeted ⁸⁹ Zr-Pertuzumab PET/CT. Radiology, 2020, 296, 370-378.	7.3	40
62	Inhibiting cancer metabolism by aromatic carbohydrate amphiphiles that act as antagonists of the glucose transporter GLUT1. Chemical Science, 2020, 11, 3737-3744.	7.4	21
63	pHâ€Responsive Polymers for Improving the Signalâ€ŧoâ€Noise Ratio of Hypoxia PET Imaging with [18 F]Fluoromisonidazole. Macromolecular Rapid Communications, 2020, 41, 2000061.	3.9	4
64	First-in-Humans Trial of Dasatinib-Derivative Tracer for Tumor Kinase-Targeted PET. Journal of Nuclear Medicine, 2020, 61, 1580-1587.	5.0	5
65	A Molecularly Targeted Intraoperative Near-Infrared Fluorescence Imaging Agent for High-Grade Serous Ovarian Cancer. Molecular Pharmaceutics, 2020, 17, 3140-3147.	4.6	10
66	Design and preclinical evaluation of nanostars for the passive pretargeting of tumor tissue. Nuclear Medicine and Biology, 2020, 84-85, 63-72.	0.6	16
67	Manipulating the In Vivo Behaviour of 68Ga with Tris(Hydroxypyridinone) Chelators: Pretargeting and Blood Clearance. International Journal of Molecular Sciences, 2020, 21, 1496.	4.1	10
68	Radiotheranostics: a roadmap for future development. Lancet Oncology, The, 2020, 21, e146-e156.	10.7	151
69	The Influence of Glycans-Specific Bioconjugation on the FcγRI Binding and <i>In vivo</i> Performance of ⁸⁹ Zr-DFO-Pertuzumab. Theranostics, 2020, 10, 1746-1757.	10.0	31
70	PET/CT Imaging with an 18F-Labeled Galactodendritic Unit in a Galectin-1–Overexpressing Orthotopic Bladder Cancer Model. Journal of Nuclear Medicine, 2020, 61, 1369-1375.	5.0	4
71	Safety and Feasibility of PARP1/2 Imaging with 18F-PARPi in Patients with Head and Neck Cancer. Clinical Cancer Research, 2020, 26, 3110-3116.	7.0	36
72	CD38-targeted Immuno-PET of Multiple Myeloma: From Xenograft Models to First-in-Human Imaging. Radiology, 2020, 295, 606-615.	7.3	73

#	Article	IF	CITATIONS
73	iNOS Regulates the Therapeutic Response of Pancreatic Cancer Cells to Radiotherapy. Cancer Research, 2020, 80, 1681-1692.	0.9	31
74	Targeted Brain Tumor Radiotherapy Using an Auger Emitter. Clinical Cancer Research, 2020, 26, 2871-2881.	7.0	69
75	HER2-Mediated Internalization of Cytotoxic Agents in <i>ERBB2</i> Amplified or Mutant Lung Cancers. Cancer Discovery, 2020, 10, 674-687.	9.4	149
76	Fluorescence labeling of a NaV1.7-targeted peptide for near-infrared nerve visualization. EJNMMI Research, 2020, 10, 49.	2.5	10
77	Demarcation of Sepsis-Induced Peripheral and Central Acidosis with pH (Low) Insertion Cycle Peptide. Journal of Nuclear Medicine, 2020, 61, 1361-1368.	5.0	12
78	The Future of Nuclear Medicine, Molecular Imaging, and Theranostics. Journal of Nuclear Medicine, 2020, 61, 263S-272S.	5.0	67
79	3D-Printable Platform for High-Throughput Small-Animal Imaging. Journal of Nuclear Medicine, 2020, 61, 1691-1692.	5.0	3
80	Biodistribution and Dosimetry of Intraventricularly Administered ¹²⁴ I-Omburtamab in Patients with Metastatic Leptomeningeal Tumors. Journal of Nuclear Medicine, 2019, 60, 1794-1801.	5.0	29
81	Improved synthesis of the bifunctional chelator <i>p</i> -SCN-Bn-HOPO. Organic and Biomolecular Chemistry, 2019, 17, 6866-6871.	2.8	12
82	Paradigms for Precision Medicine in Epichaperome Cancer Therapy. Cancer Cell, 2019, 36, 559-573.e7.	16.8	40
83	Phase I Trial of Well-Differentiated Neuroendocrine Tumors (NETs) with Radiolabeled Somatostatin Antagonist 177Lu-Satoreotide Tetraxetan. Clinical Cancer Research, 2019, 25, 6939-6947.	7.0	69
84	Retooling a Blood-Based Biomarker: Phase I Assessment of the High-Affinity CA19-9 Antibody HuMab-5B1 for Immuno-PET Imaging of Pancreatic Cancer. Clinical Cancer Research, 2019, 25, 7014-7023.	7.0	47
85	Trastuzumab gold-conjugates: synthetic approach and <i>in vitro</i> evaluation of anticancer activities in breast cancer cell lines. Chemical Communications, 2019, 55, 1394-1397.	4.1	24
86	Temporal Modulation of HER2 Membrane Availability Increases Pertuzumab Uptake and Pretargeted Molecular Imaging of Gastric Tumors. Journal of Nuclear Medicine, 2019, 60, 1569-1578.	5.0	27
87	A rapid bead-based radioligand binding assay for the determination of target-binding fraction and quality control of radiopharmaceuticals. Nuclear Medicine and Biology, 2019, 71, 32-38.	0.6	34
88	Acid specific dark quencher QC1 pHLIP for multi-spectral optoacoustic diagnoses of breast cancer. Scientific Reports, 2019, 9, 8550.	3.3	16
89	PARaDIM: A PHITS-Based Monte Carlo Tool for Internal Dosimetry with Tetrahedral Mesh Computational Phantoms. Journal of Nuclear Medicine, 2019, 60, 1802-1811.	5.0	27

90 Molecular Imaging Companion Diagnostics. , 2019, , 201-228.

#	Article	IF	CITATIONS
91	Toward the Optimization of Click-Mediated Pretargeted Radioimmunotherapy. Molecular Pharmaceutics, 2019, 16, 2259-2263.	4.6	19
92	Assessment of Simplified Methods for Quantification of 18F-FDHT Uptake in Patients with Metastatic Castration-Resistant Prostate Cancer. Journal of Nuclear Medicine, 2019, 60, 1221-1227.	5.0	10
93	<i>EGFR</i> and <i>MET</i> Amplifications Determine Response to HER2 Inhibition in <i>ERBB2</i> -Amplified Esophagogastric Cancer. Cancer Discovery, 2019, 9, 199-209.	9.4	115
94	Nanobody-Facilitated Multiparametric PET/MRI Phenotyping of Atherosclerosis. JACC: Cardiovascular Imaging, 2019, 12, 2015-2026.	5.3	66
95	Leveraging Bioorthogonal Click Chemistry to Improve 225Ac-Radioimmunotherapy of Pancreatic Ductal Adenocarcinoma. Clinical Cancer Research, 2019, 25, 868-880.	7.0	55
96	Biodistribution and radiation dose estimates for 68Ga-DOTA-JR11 in patients with metastatic neuroendocrine tumors. European Journal of Nuclear Medicine and Molecular Imaging, 2019, 46, 677-685.	6.4	44
97	Harnessing Androgen Receptor Pathway Activation for Targeted Alpha Particle Radioimmunotherapy of Breast Cancer. Clinical Cancer Research, 2019, 25, 881-891.	7.0	21
98	A PET Imaging Strategy for Interrogating Target Engagement and Oncogene Status in Pancreatic Cancer. Clinical Cancer Research, 2019, 25, 166-176.	7.0	14
99	Tumor-Specific Zr-89 Immuno-PET Imaging in a Human Bladder Cancer Model. Molecular Imaging and Biology, 2018, 20, 808-815.	2.6	22
100	Click-Mediated Pretargeted Radioimmunotherapy of Colorectal Carcinoma. Molecular Pharmaceutics, 2018, 15, 1729-1734.	4.6	36
101	Imaging of human epidermal growth factor receptors for patient selection and response monitoring – From PET imaging and beyond. Cancer Letters, 2018, 419, 139-151.	7.2	26
102	α-Emitters for Radiotherapy: From Basic Radiochemistry to Clinical Studies—Part 2. Journal of Nuclear Medicine, 2018, 59, 1020-1027.	5.0	72
103	Feed-forward alpha particle radiotherapy ablates androgen receptor-addicted prostate cancer. Nature Communications, 2018, 9, 1629.	12.8	37
104	Reproducibility and Repeatability of Semiquantitative ¹⁸ F-Fluorodihydrotestosterone Uptake Metrics in Castration-Resistant Prostate Cancer Metastases: A Prospective Multicenter Study. Journal of Nuclear Medicine, 2018, 59, 1516-1523.	5.0	20
105	In Vivo PET Assay of Tumor Glutamine Flux and Metabolism: In-Human Trial of ¹⁸ F-(2 <i>S</i> ,4 <i>R</i>)-4-Fluoroglutamine. Radiology, 2018, 287, 667-675.	7.3	80
106	The inverse electron-demand Diels–Alder reaction as a new methodology for the synthesis of225Ac-labelled radioimmunoconjugates. Chemical Communications, 2018, 54, 2599-2602.	4.1	33
107	Bioorthogonal Masking of Circulating Antibody–TCO Groups Using Tetrazine-Functionalized Dextran Polymers. Bioconjugate Chemistry, 2018, 29, 538-545.	3.6	35
108	Preclinical optimization of antibodyâ€based radiopharmaceuticals for cancer imaging and radionuclide therapy—Model, vector, and radionuclide selection. Journal of Labelled Compounds and Radiopharmaceuticals, 2018, 61, 611-635.	1.0	24

#	Article	IF	CITATIONS
109	Fc-Mediated Anomalous Biodistribution of Therapeutic Antibodies in Immunodeficient Mouse Models. Cancer Research, 2018, 78, 1820-1832.	0.9	69
110	PARP-1–Targeted Radiotherapy in Mouse Models of Glioblastoma. Journal of Nuclear Medicine, 2018, 59, 1225-1233.	5.0	51
111	α-Emitters for Radiotherapy: From Basic Radiochemistry to Clinical Studies—Part 1. Journal of Nuclear Medicine, 2018, 59, 878-884.	5.0	131
112	Pharmacokinetics, Biodistribution, and Radiation Dosimetry for ⁸⁹ Zr-Trastuzumab in Patients with Esophagogastric Cancer. Journal of Nuclear Medicine, 2018, 59, 161-166.	5.0	96
113	Biodistribution and Dosimetry of ¹⁸ F-Meta-Fluorobenzylguanidine: A First-in-Human PET/CT Imaging Study of Patients with Neuroendocrine Malignancies. Journal of Nuclear Medicine, 2018, 59, 147-153.	5.0	96
114	A phase II study of radioimmunotherapy with intraventricular ¹³¹ lâ€3F8 for medulloblastoma. Pediatric Blood and Cancer, 2018, 65, e26754.	1.5	46
115	Noninvasive ⁸⁹ Zr-Transferrin PET Shows Improved Tumor Targeting Compared with ¹⁸ F-FDG PET in MYC-Overexpressing Human Triple-Negative Breast Cancer. Journal of Nuclear Medicine, 2018, 59, 51-57.	5.0	31
116	Long–Half-Life ⁸⁹ Zr-Labeled Radiotracers Can Guide Percutaneous Biopsy Within the PET/CT Suite Without Reinjection of Radiotracer. Journal of Nuclear Medicine, 2018, 59, 399-402.	5.0	9
117	First-in-Human Human Epidermal Growth Factor Receptor 2–Targeted Imaging Using ⁸⁹ Zr-Pertuzumab PET/CT: Dosimetry and Clinical Application in Patients with Breast Cancer. Journal of Nuclear Medicine, 2018, 59, 900-906.	5.0	126
118	Positron Emission Tomography/Computed Tomography–Based Assessments of Androgen Receptor Expression and Glycolytic Activity as a Prognostic Biomarker for Metastatic Castration-Resistant Prostate Cancer. JAMA Oncology, 2018, 4, 217.	7.1	93
119	Leveraging PET to image folate receptor $\hat{I}\pm$ therapy of an antibody-drug conjugate. EJNMMI Research, 2018, 8, 87.	2.5	12
120	Caveolin-1 mediates cellular distribution of HER2 and affects trastuzumab binding and therapeutic efficacy. Nature Communications, 2018, 9, 5137.	12.8	78
121	Clinical Potential of Human Epidermal Growth Factor Receptor 2 and Human Epidermal Growth Factor Receptor 3 Imaging in Breast Cancer. PET Clinics, 2018, 13, 423-435.	3.0	21
122	Convection-enhanced delivery for diffuse intrinsic pontine glioma: a single-centre, dose-escalation, phase 1 trial. Lancet Oncology, The, 2018, 19, 1040-1050.	10.7	201
123	Imaging EGFR and HER3 through 89Zr-labeled MEHD7945A (Duligotuzumab). Scientific Reports, 2018, 8, 9043.	3.3	17
124	Establishment of the <i>In Vivo</i> Efficacy of Pretargeted Radioimmunotherapy Utilizing Inverse Electron Demand Diels-Alder Click Chemistry. Molecular Cancer Therapeutics, 2017, 16, 124-133.	4.1	79
125	⁸⁹ Zr-DFO-AMG102 Immuno-PET to Determine Local Hepatocyte Growth Factor Protein Levels in Tumors for Enhanced Patient Selection. Journal of Nuclear Medicine, 2017, 58, 1386-1394.	5.0	33
126	Preloading with Unlabeled CA19.9 Targeted Human Monoclonal Antibody Leads to Improved PET Imaging with ⁸⁹ Zr-5B1. Molecular Pharmaceutics, 2017, 14, 908-915.	4.6	31

#	Article	IF	CITATIONS
127	Applications of pHLIP Technology for Cancer Imaging and Therapy. Trends in Biotechnology, 2017, 35, 653-664.	9.3	90
128	Noninvasive Interrogation of DLL3 Expression in Metastatic Small Cell Lung Cancer. Cancer Research, 2017, 77, 3931-3941.	0.9	91
129	Antibodies Against Specific MUC16 Glycosylation Sites Inhibit Ovarian Cancer Growth. ACS Chemical Biology, 2017, 12, 2085-2096.	3.4	32
130	Human Epidermal Growth Factor Receptor 2-Targeted PET/Single- Photon Emission Computed Tomography Imaging of Breast Cancer. PET Clinics, 2017, 12, 269-288.	3.0	49
131	Multinuclear NMR and MRI Reveal an Early Metabolic Response to mTOR Inhibition in Sarcoma. Cancer Research, 2017, 77, 3113-3120.	0.9	18
132	Noninvasive Measurement of mTORC1 Signaling with 89Zr-Transferrin. Clinical Cancer Research, 2017, 23, 3045-3052.	7.0	31
133	Current status and future challenges for molecular imaging. Philosophical Transactions Series A, Mathematical, Physical, and Engineering Sciences, 2017, 375, 20170023.	3.4	22
134	Targeted PET imaging strategy to differentiate malignant from inflamed lymph nodes in diffuse large B-cell lymphoma. Proceedings of the National Academy of Sciences of the United States of America, 2017, 114, E7441-E7449.	7.1	28
135	Multiplexed imaging for diagnosis and therapy. Nature Biomedical Engineering, 2017, 1, 697-713.	22.5	133
136	Exploring Structural Parameters for Pretargeting Radioligand Optimization. Journal of Medicinal Chemistry, 2017, 60, 8201-8217.	6.4	52
137	89Zr-Trastuzumab PET/CT for Detection of Human Epidermal Growth Factor Receptor 2–Positive Metastases in Patients With Human Epidermal Growth Factor Receptor 2–Negative Primary Breast Cancer. Clinical Nuclear Medicine, 2017, 42, 912-917.	1.3	81
138	Prospective Clinical Trial of ¹⁸ F-Fluciclovine PET/CT for Determining the Response to Neoadjuvant Therapy in Invasive Ductal and Invasive Lobular Breast Cancers. Journal of Nuclear Medicine, 2017, 58, 1037-1042.	5.0	47
139	Imaging biomarker roadmap for cancer studies. Nature Reviews Clinical Oncology, 2017, 14, 169-186.	27.6	792
140	Pretargeting of internalizing trastuzumab and cetuximab with a 18F-tetrazine tracer in xenograft models. EJNMMI Research, 2017, 7, 95.	2.5	58
141	Novel Positron-Emitting Radiopharmaceuticals. , 2017, , 129-171.		0
142	A Pretargeted Approach for the Multimodal PET/NIRF Imaging of Colorectal Cancer. Theranostics, 2016, 6, 2267-2277.	10.0	53
143	Pretargeted PET Imaging Using a Site-Specifically Labeled Immunoconjugate. Bioconjugate Chemistry, 2016, 27, 1789-1795.	3.6	60
144	Radiosynthesis of the iodineâ€124 labeled Hsp90 inhibitor PUâ€H71. Journal of Labelled Compounds and Radiopharmaceuticals, 2016, 59, 129-132.	1.0	17

#	Article	IF	CITATIONS
145	Nanoreporter PET predicts the efficacy of anti-cancer nanotherapy. Nature Communications, 2016, 7, 11838.	12.8	94
146	Internalization of secreted antigen–targeted antibodies by the neonatal Fc receptor for precision imaging of the androgen receptor axis. Science Translational Medicine, 2016, 8, 367ra167.	12.4	23
147	Molecular Imaging of Ovarian Cancer. Journal of Nuclear Medicine, 2016, 57, 827-833.	5.0	17
148	Detection of HER2-Positive Metastases in Patients with HER2-Negative Primary Breast Cancer Using ⁸⁹ Zr-Trastuzumab PET/CT. Journal of Nuclear Medicine, 2016, 57, 1523-1528.	5.0	146
149	The epichaperome is an integrated chaperome network that facilitates tumour survival. Nature, 2016, 538, 397-401.	27.8	233
150	Selective Imaging of VEGFR-1 and VEGFR-2 Using ⁸⁹ Zr-Labeled Single-Chain VEGF Mutants. Journal of Nuclear Medicine, 2016, 57, 1811-1816.	5.0	21
151	Fully automated synthesis of [¹⁸ F]fluoroâ€dihydrotestosterone ([¹⁸ F]FDHT) using the FlexLab module. Journal of Labelled Compounds and Radiopharmaceuticals, 2016, 59, 424-428.	1.0	10
152	First-in-Human Imaging with ⁸⁹ Zr-Df-IAB2M Anti-PSMA Minibody in Patients with Metastatic Prostate Cancer: Pharmacokinetics, Biodistribution, Dosimetry, and Lesion Uptake. Journal of Nuclear Medicine, 2016, 57, 1858-1864.	5.0	116
153	PET Imaging of Extracellular pH in Tumors with ⁶⁴ Cu- and ¹⁸ F-Labeled pHLIP Peptides: A Structure–Activity Optimization Study. Bioconjugate Chemistry, 2016, 27, 2014-2023.	3.6	52
154	A comparative evaluation of the chelators H 4 octapa and CHX-A″-DTPA with the therapeutic radiometal 90 Y. Nuclear Medicine and Biology, 2016, 43, 566-576.	0.6	25
155	Emerging Radiopharmaceuticals in Clinical Oncology. , 2016, , 1-43.		0
156	Click Chemistry and Radiochemistry: The First 10 Years. Bioconjugate Chemistry, 2016, 27, 2791-2807.	3.6	197
157	Synthesis and evaluation of an 18 F-labeled pyrimidine-pyridine amine for targeting CXCR4 receptors in gliomas. Nuclear Medicine and Biology, 2016, 43, 606-611.	0.6	12
158	InÂVivo PET Imaging of HDL in MultipleÂAtherosclerosisÂModels. JACC: Cardiovascular Imaging, 2016, 9, 950-961.	5.3	78
159	Applying ⁸⁹ Zr-Transferrin To Study the Pharmacology of Inhibitors to BET Bromodomain Containing Proteins. Molecular Pharmaceutics, 2016, 13, 683-688.	4.6	12
160	Preclinical ⁸⁹ Zr Immuno-PET of High-Grade Serous Ovarian Cancer and Lymph Node Metastasis. Journal of Nuclear Medicine, 2016, 57, 771-776.	5.0	31
161	Initial Results of a Prospective Clinical Trial of ¹⁸ F-Fluciclovine PET/CT in Newly Diagnosed Invasive Ductal and Invasive Lobular Breast Cancers. Journal of Nuclear Medicine, 2016, 57, 1350-1356.	5.0	60
162	¹⁸ F-Based Pretargeted PET Imaging Based on Bioorthogonal Diels–Alder Click Chemistry. Bioconjugate Chemistry, 2016, 27, 298-301.	3.6	127

#	Article	IF	CITATIONS
163	Pretargeted Immuno-PET of Pancreatic Cancer: Overcoming Circulating Antigen and Internalized Antibody to Reduce Radiation Doses. Journal of Nuclear Medicine, 2016, 57, 453-459.	5.0	80
164	Novel Positron Emitting Radiopharmaceuticals. , 2016, , 1-43.		0
165	Challenges of Pancreatic Cancer. Cancer Journal (Sudbury, Mass), 2015, 21, 188-193.	2.0	44
166	Glutamine-based PET imaging facilitates enhanced metabolic evaluation of gliomas in vivo. Science Translational Medicine, 2015, 7, 274ra17.	12.4	257
167	Harnessing the Bioorthogonal Inverse Electron Demand Diels-Alder Cycloaddition for Pretargeted PET Imaging. Journal of Visualized Experiments, 2015, , e52335.	0.3	6
168	Low incidence of radionecrosis in children treated with conventional radiation therapy and intrathecal radioimmunotherapy. Journal of Neuro-Oncology, 2015, 123, 245-249.	2.9	22
169	Site-specifically labeled CA19.9-targeted immunoconjugates for the PET, NIRF, and multimodal PET/NIRF imaging of pancreatic cancer. Proceedings of the National Academy of Sciences of the United States of America, 2015, 112, 15850-15855.	7.1	85
170	Evaluation of Hypoxia With Copper-Labeled Diacetyl-bis(N-Methylthiosemicarbazone). Seminars in Nuclear Medicine, 2015, 45, 177-185.	4.6	34
171	Fully-automated synthesis of 16β- 18 F-fluoro-5α-dihydrotestosterone (FDHT) on the ELIXYS radiosynthesizer. Applied Radiation and Isotopes, 2015, 103, 9-14.	1.5	10
172	PET Imaging of Tumor-Associated Macrophages with ⁸⁹ Zr-Labeled High-Density Lipoprotein Nanoparticles. Journal of Nuclear Medicine, 2015, 56, 1272-1277.	5.0	145
173	PI3K inhibition results in enhanced estrogen receptor function and dependence in hormone receptor–positive breast cancer. Science Translational Medicine, 2015, 7, 283ra51.	12.4	276
174	A Phase I/II Study for Analytic Validation of 89Zr-J591 ImmunoPET as a Molecular Imaging Agent for Metastatic Prostate Cancer. Clinical Cancer Research, 2015, 21, 5277-5285.	7.0	163
175	Precision Medicine…Visualized—a Message from the President of the WMIC. Molecular Imaging and Biology, 2015, 17, 443-444.	2.6	Ο
176	Androgen Receptor Upregulation Mediates Radioresistance after Ionizing Radiation. Cancer Research, 2015, 75, 4688-4696.	0.9	105
177	Optimization of a Pretargeted Strategy for the PET Imaging of Colorectal Carcinoma via the Modulation of Radioligand Pharmacokinetics. Molecular Pharmaceutics, 2015, 12, 3575-3587.	4.6	88
178	<i>p</i> -SCN-Bn-HOPO: A Superior Bifunctional Chelator for ⁸⁹ Zr ImmunoPET. Bioconjugate Chemistry, 2015, 26, 2579-2591.	3.6	104
179	The Bioconjugation and Radiosynthesis of ⁸⁹ Zr-DFO-labeled Antibodies. Journal of Visualized Experiments, 2015, , .	0.3	60
180	89Zr-huJ591 immuno-PET imaging in patients with advanced metastatic prostate cancer. European Journal of Nuclear Medicine and Molecular Imaging, 2014, 41, 2093-2105.	6.4	130

#	Article	IF	CITATIONS
181	Annotating STEAP1 Regulation in Prostate Cancer with 89Zr Immuno-PET. Journal of Nuclear Medicine, 2014, 55, 2045-2049.	5.0	25
182	Antagonism of EGFR and HER3 Enhances the Response to Inhibitors of the PI3K-Akt Pathway in Triple-Negative Breast Cancer. Science Signaling, 2014, 7, ra29.	3.6	123
183	Building Blocks for the Construction of Bioorthogonally Reactive Peptides via Solidâ€Phase Peptide Synthesis. ChemistryOpen, 2014, 3, 48-53.	1.9	24
184	Chemoenzymatic Strategy for the Synthesis of Site-Specifically Labeled Immunoconjugates for Multimodal PET and Optical Imaging. Bioconjugate Chemistry, 2014, 25, 2123-2128.	3.6	64
185	Understanding the pharmacological properties of a metabolic PET tracer in prostate cancer. Proceedings of the National Academy of Sciences of the United States of America, 2014, 111, 7254-7259.	7.1	40
186	Imaging the Norepinephrine Transporter in Neuroblastoma: A Comparison of [18F]-MFBG and 123I-MIBG. Clinical Cancer Research, 2014, 20, 2182-2191.	7.0	61
187	Distant metastasis in p16-positive oropharyngeal squamous cell carcinoma: A critical analysis of patterns and outcomes. Oral Oncology, 2014, 50, 45-51.	1.5	81
188	Synthesis and evaluation of 18F-labeled benzylguanidine analogs for targeting the human norepinephrine transporter. European Journal of Nuclear Medicine and Molecular Imaging, 2014, 41, 322-332.	6.4	50
189	H6phospa-trastuzumab: bifunctional methylenephosphonate-based chelator with89Zr,111In and177Lu. Dalton Transactions, 2014, 43, 119-131.	3.3	57
190	Underscoring the Influence of Inorganic Chemistry on Nuclear Imaging with Radiometals. Inorganic Chemistry, 2014, 53, 1880-1899.	4.0	75
191	Noninvasive Imaging of PSMA in Prostate Tumors with ⁸⁹ Zr-Labeled huJ591 Engineered Antibody Fragments: The Faster Alternatives. Molecular Pharmaceutics, 2014, 11, 3965-3973.	4.6	65
192	A Modular Labeling Strategy for In Vivo PET and Near-Infrared Fluorescence Imaging of Nanoparticle Tumor Targeting. Journal of Nuclear Medicine, 2014, 55, 1706-1711.	5.0	85
193	Targeting Breast Tumors with pH (Low) Insertion Peptides. Molecular Pharmaceutics, 2014, 11, 2896-2905.	4.6	57
194	Pairwise comparison of 89Zr- and 124I-labeled cG250 based on positron emission tomography imaging and nonlinear immunokinetic modeling: in vivo carbonic anhydrase IX receptor binding and internalization in mouse xenografts of clear-cell renal cell carcinoma. European Journal of Nuclear Medicine and Molecular Imaging, 2014, 41, 985-994.	6.4	65
195	Alternative Chelator for ⁸⁹ Zr Radiopharmaceuticals: Radiolabeling and Evaluation of 3,4,3-(LI-1,2-HOPO). Journal of Medicinal Chemistry, 2014, 57, 4849-4860.	6.4	143
196	Synthesis and evaluation of 18F-labeled ATP competitive inhibitors of topoisomerase II as probes for imaging topoisomerase II expression. European Journal of Medicinal Chemistry, 2014, 86, 769-781.	5.5	9
197	What a Difference a Carbon Makes: H ₄ octapa vs H ₄ C3octapa, Ligands for In-111 and Lu-177 Radiochemistry. Inorganic Chemistry, 2014, 53, 10412-10431.	4.0	38
198	CDK9-mediated transcription elongation is required for MYC addiction in hepatocellular carcinoma. Genes and Development, 2014, 28, 1800-1814.	5.9	167

#	Article	IF	CITATIONS
199	A Prospective Pilot Study of ⁸⁹ Zr-J591/Prostate Specific Membrane Antigen Positron Emission Tomography in Men with Localized Prostate Cancer Undergoing Radical Prostatectomy. Journal of Urology, 2014, 191, 1439-1445.	0.4	73
200	Influence of free fatty acids on glucose uptake in prostate cancer cells. Nuclear Medicine and Biology, 2014, 41, 254-258.	0.6	9
201	Development of a minimal saponin vaccine adjuvant based on QS-21. Nature Chemistry, 2014, 6, 635-643.	13.6	68
202	89Zr-Labeled Paramagnetic Octreotide-Liposomes for PET-MR Imaging of Cancer. Pharmaceutical Research, 2013, 30, 878-888.	3.5	81
203	Antilipolytic drug boosts glucose metabolism in prostate cancer. Nuclear Medicine and Biology, 2013, 40, 524-528.	0.6	5
204	Sandmeyer reaction repurposed for the site-selective, non-oxidizing radioiodination of fully-deprotected peptides: Studies on the endogenous opioid peptide α-neoendorphin. Bioorganic and Medicinal Chemistry Letters, 2013, 23, 4347-4350.	2.2	11
205	¹⁸ F-Labeled-Bioorthogonal Liposomes for <i>In Vivo</i> Targeting. Bioconjugate Chemistry, 2013, 24, 1784-1789.	3.6	74
206	Radiopharmaceuticals for Imaging in Oncology with Special Emphasis on Positron-Emitting Agents. , 2013, , 35-78.		2
207	PET imaging with 89Zr: From radiochemistry to the clinic. Nuclear Medicine and Biology, 2013, 40, 3-14.	0.6	338
208	Imaging Tumor Burden in the Brain with ⁸⁹ Zr-Transferrin. Journal of Nuclear Medicine, 2013, 54, 90-95.	5.0	33
209	Monitoring Afatinib Treatment in HER2-Positive Gastric Cancer with 18F-FDG and 89Zr-Trastuzumab PET. Journal of Nuclear Medicine, 2013, 54, 936-943.	5.0	85
210	Enzyme-Mediated Methodology for the Site-Specific Radiolabeling of Antibodies Based on Catalyst-Free Click Chemistry. Bioconjugate Chemistry, 2013, 24, 1057-1067.	3.6	123
211	H ₄ octapa-Trastuzumab: Versatile Acyclic Chelate System for ¹¹¹ In and ¹⁷⁷ Lu Imaging and Therapy. Journal of the American Chemical Society, 2013, 135, 12707-12721.	13.7	82
212	Feasibility and Predictability of Perioperative PET and Estrogen Receptor Ligand in Patients with Invasive Breast Cancer. Journal of Nuclear Medicine, 2013, 54, 1697-1702.	5.0	64
213	A Pretargeted PET Imaging Strategy Based on Bioorthogonal Diels–Alder Click Chemistry. Journal of Nuclear Medicine, 2013, 54, 1389-1396.	5.0	247
214	The Growing Impact of Bioorthogonal Click Chemistry on the Development of Radiopharmaceuticals. Journal of Nuclear Medicine, 2013, 54, 829-832.	5.0	108
215	Applying PET to Broaden the Diagnostic Utility of the Clinically Validated CA19.9 Serum Biomarker for Oncology. Journal of Nuclear Medicine, 2013, 54, 1876-1882.	5.0	58
216	Fatty Acid Synthase Is a Key Target in Multiple Essential Tumor Functions of Prostate Cancer: Uptake of Radiolabeled Acetate as a Predictor of the Targeted Therapy Outcome. PLoS ONE, 2013, 8, e64570.	2.5	88

#	Article	IF	CITATIONS
217	Imaging Androgen Receptor Signaling with a Radiotracer Targeting Free Prostate-Specific Antigen. Cancer Discovery, 2012, 2, 320-327.	9.4	68
218	Annotating MYC status with 89Zr-transferrin imaging. Nature Medicine, 2012, 18, 1586-1591.	30.7	83
219	Efficient ¹⁸ F-Labeling of Large 37-Amino-Acid pHLIP Peptide Analogues and Their Biological Evaluation. Bioconjugate Chemistry, 2012, 23, 1557-1566.	3.6	60
220	An improved strategy for the synthesis of [18F]-labeled arabinofuranosyl nucleosides. Nuclear Medicine and Biology, 2012, 39, 1182-1188.	0.6	10
221	H ₂ azapa: a Versatile Acyclic Multifunctional Chelator for ⁶⁷ Ga, ⁶⁴ Cu, ¹¹¹ In, and ¹⁷⁷ Lu. Inorganic Chemistry, 2012, 51, 12575-12589.	4.0	52
222	Preface: 14th International Workshop on Targetry and Target Chemistry (WTTC). , 2012, , .		0
223	Dosimetry of 18F-Labeled Tyrosine Kinase Inhibitor SKI-249380, a Dasatinib-Tracer for PET Imaging. Molecular Imaging and Biology, 2012, 14, 25-31.	2.6	10
224	Modular Strategy for the Construction of Radiometalated Antibodies for Positron Emission Tomography Based on Inverse Electron Demand Diels–Alder Click Chemistry. Bioconjugate Chemistry, 2011, 22, 2048-2059.	3.6	142
225	⁸⁹ Zr-Labeled Dextran Nanoparticles Allow in Vivo Macrophage Imaging. Bioconjugate Chemistry, 2011, 22, 2383-2389.	3.6	116
226	Role of Metalation in the Topoisomerase IIα Inhibition and Antiproliferation Activity of a Series of α-Heterocyclic-N ⁴ -Substituted Thiosemicarbazones and Their Cu(II) Complexes. Journal of Medicinal Chemistry, 2011, 54, 2391-2398.	6.4	168
227	A practical guide to the construction of radiometallated bioconjugates for positron emission tomography. Dalton Transactions, 2011, 40, 6168.	3.3	169
228	The synthesis and evaluation of N1-(4-(2-[18F]-fluoroethyl)phenyl)-N8-hydroxyoctanediamide ([18F]-FESAHA), A PET radiotracer designed for the delineation of histone deacetylase expression in cancer. Nuclear Medicine and Biology, 2011, 38, 683-696.	0.6	18
229	The Next Generation of Positron Emission Tomography Radiopharmaceuticals in Oncology. Seminars in Nuclear Medicine, 2011, 41, 265-282.	4.6	93
230	Intraoperative Imaging of Positron Emission Tomographic Radiotracers Using Cerenkov Luminescence Emissions. Molecular Imaging, 2011, 10, 7290.2010.00047.	1.4	53
231	Intraoperative Imaging of Positron Emission Tomographic Radiotracers Using Cerenkov Luminescence Emissions. Molecular Imaging, 2011, 10, 7290.2010.00047.	1.4	44
232	Ex vivo sentinel lymph node mapping in laparoscopic resection of colon cancer. Colorectal Disease, 2011, 13, 1249-1255.	1.4	7
233	Targeting the Internal Epitope of Prostate-Specific Membrane Antigen with ⁸⁹ Zr-7E11 Immuno-PET. Journal of Nuclear Medicine, 2011, 52, 1608-1615.	5.0	56
234	Magnitude of Enhanced Permeability and Retention Effect in Tumors with Different Phenotypes: ⁸⁹ Zr-Albumin as a Model System. Journal of Nuclear Medicine, 2011, 52, 625-633.	5.0	144

#	Article	IF	CITATIONS
235	Affinity-based proteomics reveal cancer-specific networks coordinated by Hsp90. Nature Chemical Biology, 2011, 7, 818-826.	8.0	240
236	Intraoperative imaging of positron emission tomographic radiotracers using Cerenkov luminescence emissions. Molecular Imaging, 2011, 10, 177-86, 1-3.	1.4	58
237	Unconventional Nuclides for Radiopharmaceuticals. Molecular Imaging, 2010, 9, 7290.2010.00008.	1.4	126
238	Nitroimidazole conjugates of bis(thiosemicarbazonato)64Cu(II) – Potential combination agents for the PET imaging of hypoxia. Journal of Inorganic Biochemistry, 2010, 104, 126-135.	3.5	50
239	Imaging and treating tumor vasculature with targeted radiolabeled carbon nanotubes. International Journal of Nanomedicine, 2010, 5, 783.	6.7	117
240	Measuring the Pharmacodynamic Effects of a Novel Hsp90 Inhibitor on HER2/neu Expression in Mice Using 89Zr-DFO-Trastuzumab. PLoS ONE, 2010, 5, e8859.	2.5	121
241	Cerenkov Luminescence Imaging of Medical Isotopes. Journal of Nuclear Medicine, 2010, 51, 1123-1130.	5.0	279
242	⁸⁹ Zr-DFO-J591 for ImmunoPET of Prostate-Specific Membrane Antigen Expression In Vivo. Journal of Nuclear Medicine, 2010, 51, 1293-1300.	5.0	373
243	Improved synthesis of 2′-deoxy-2′-[18F]-fluoro-1-β-d-arabinofuranosyl-5-iodouracil ([18F]-FIAU). Nuclear Medicine and Biology, 2010, 37, 439-442.	0.6	32
244	Clickable bifunctional radiometal chelates for peptide labeling. Chemical Communications, 2010, 46, 1706.	4.1	43
245	Unconventional nuclides for radiopharmaceuticals. Molecular Imaging, 2010, 9, 1-20.	1.4	52
246	In Vivo Biodistribution, PET Imaging, and Tumor Accumulation of ⁸⁶ Y- and ¹¹¹ In-Antimindin/RG-1, Engineered Antibody Fragments in LNCaP Tumor–Bearing Nude Mice. Journal of Nuclear Medicine, 2009, 50, 435-443.	5.0	76
247	Radiopharmaceuticals in Preclinical and Clinical Development for Monitoring of Therapy with PET. Journal of Nuclear Medicine, 2009, 50, 106S-121S.	5.0	92
248	A Novel Technology for the Imaging of Acidic Prostate Tumors by Positron Emission Tomography. Cancer Research, 2009, 69, 4510-4516.	0.9	154
249	Bromination from the Macroscopic Level to the Tracer Radiochemical Level:76Br Radiolabeling of Aromatic Compounds via Electrophilic Substitution. Bioconjugate Chemistry, 2009, 20, 808-816.	3.6	14
250	64Cu-Labeled CB-TE2A and diamsar-conjugated RGD peptide analogs for targeting angiogenesis: comparison of their biological activity. Nuclear Medicine and Biology, 2009, 36, 277-285.	0.6	87
251	Melanoma imaging using 111In-, 86Y- and 68Ga-labeled CHX-A″-Re(Arg11)CCMSH. Nuclear Medicine and Biology, 2009, 36, 345-354.	0.6	53
252	Standardized methods for the production of high specific-activity zirconium-89. Nuclear Medicine and Biology, 2009, 36, 729-739.	0.6	369

#	Article	IF	CITATIONS
253	Functionalised copper-64 complexes as precursors of potential PET imaging agents for neurodegenerative disorders. New Journal of Chemistry, 2009, 33, 1845.	2.8	7
254	Synthesis and characterization of the copper(ii) complexes of new N2S2-donor macrocyclic ligands: synthesis and in vivo evaluation of the64Cu complexes. Dalton Transactions, 2009, , 177-184.	3.3	15
255	Copper-64 Radiopharmaceuticals for Oncologic Imaging. PET Clinics, 2009, 4, 49-67.	3.0	14
256	Assessing tumor hypoxia by positron emission tomography with Cu-ATSM. Quarterly Journal of Nuclear Medicine and Molecular Imaging, 2009, 53, 193-200.	0.7	56
257	Synthesis, in vitro and in vivo characterization of 64Cu(l) complexes derived from hydrophilic tris(hydroxymethyl)phosphane and 1,3,5-triaza-7-phosphaadamantane ligands. Journal of Biological Inorganic Chemistry, 2008, 13, 307-315.	2.6	46
258	Tumor Hypoxia Detected by Positron Emission Tomography with 60Cu-ATSM as a Predictor of Response and Survival in Patients Undergoing Neoadjuvant Chemoradiotherapy for Rectal Carcinoma: A Pilot Study. Diseases of the Colon and Rectum, 2008, 51, 1641-1648.	1.3	151
259	In Vitro and In Vivo Evaluation of Bifunctional Bisthiosemicarbazone ⁶⁴ Cu-Complexes for the Positron Emission Tomography Imaging of Hypoxia. Journal of Medicinal Chemistry, 2008, 51, 2985-2991.	6.4	72
260	Examining the relationship between Cu-ATSM hypoxia selectivity and fatty acid synthase expression in human prostate cancer cell lines. Nuclear Medicine and Biology, 2008, 35, 273-279.	0.6	51
261	Evaluation of a bromine-76-labeled progestin 16α,17α-dioxolane for breast tumor imaging and radiotherapy: in vivo biodistribution and metabolic stability studies. Nuclear Medicine and Biology, 2008, 35, 655-663.	0.6	16
262	Autoradiographic and small-animal PET comparisons between 18F-FMISO, 18F-FDG, 18F-FLT and the hypoxic selective 64Cu-ATSM in a rodent model of cancer. Nuclear Medicine and Biology, 2008, 35, 713-720.	0.6	82
263	An Imaging Comparison of ⁶⁴ Cu-ATSM and ⁶⁰ Cu-ATSM in Cancer of the Uterine Cervix. Journal of Nuclear Medicine, 2008, 49, 1177-1182.	5.0	178
264	1- ¹¹ C-Acetate as a PET Radiopharmaceutical for Imaging Fatty Acid Synthase Expression in Prostate Cancer. Journal of Nuclear Medicine, 2008, 49, 327-334.	5.0	152
265	Assessing Tumor Hypoxia in Cervical Cancer by PET with ⁶⁰ Cu-Labeled Diacetyl-Bis(<i>N</i> ⁴ -Methylthiosemicarbazone). Journal of Nuclear Medicine, 2008, 49, 201-205.	5.0	221
266	SU-GC-J-03: 3D Pathology Validation for Head-And-Neck Tumor Segmentation in PET/CT/MRI Images. Medical Physics, 2008, 35, 2679-2679.	3.0	0
267	NuMA Influences Higher Order Chromatin Organization in Human Mammary Epithelium. Molecular Biology of the Cell, 2007, 18, 348-361.	2.1	64
268	IN VIVO IMAGING IN A MURINE MODEL OF GLIOBLASTOMA. Neurosurgery, 2007, 60, 360-371.	1.1	37
269	Gallium-68-labeled DOTA-rhenium-cyclized α-melanocyte-stimulating hormone analog for imaging of malignant melanoma. Nuclear Medicine and Biology, 2007, 34, 945-953.	0.6	47
270	An Anatomical Study of Tibial Metaphyseal/Diaphyseal Mismatch During Revision Total Knee Arthroplasty. Journal of Arthroplasty, 2007, 22, 241-244.	3.1	27

#	Article	IF	CITATIONS
271	Cu–ATSM: A radiopharmaceutical for the PET imaging of hypoxia. Dalton Transactions, 2007, , 4893.	3.3	213
272	Molecular Imaging of Gastrin-Releasing Peptide Receptor-Positive Tumors in Mice Using ⁶⁴ Cu- and ⁸⁶ Y-DOTAâ^'(Pro ¹ ,Tyr ⁴)-Bombesin(1â^'14). Bioconjugate Chemistry, 2007, 18, 724-730.	3.6	65
273	Imaging oxygenation of human tumours. European Radiology, 2007, 17, 861-872.	4.5	304
274	Diagnostic and prognostic value of ambulatory ECG (Holter) monitoring in patients with coronary heart disease: a review. Journal of Thrombosis and Thrombolysis, 2007, 23, 135-145.	2.1	27
275	Radiometal-Labeled Somatostatin Analogs for Applications in Cancer Imaging and Therapy. Methods in Molecular Biology, 2007, 386, 227-240.	0.9	18
276	Production of Non-standard PET Radionuclides and the Application of Radiopharmaceuticals Labeled with these Nuclides. , 2007, , 159-181.		16
277	Synthesis and biologic evaluation of 64Cu-labeled rhenium-cyclized alpha-MSH peptide analog using a cross-bridged cyclam chelator. Journal of Nuclear Medicine, 2007, 48, 64-72.	5.0	57
278	Hypoxia: Importance in tumor biology, noninvasive measurement by imaging, and value of its measurement in the management of cancer therapy. International Journal of Radiation Biology, 2006, 82, 699-757.	1.8	561
279	Validation of a Novel CHX-Aâ€~Ââ€~ Derivative Suitable for Peptide Conjugation: Small Animal PET/CT Imaging Using Yttrium-86-CHX-A†Ââ€~-Octreotide. Journal of Medicinal Chemistry, 2006, 49, 4297-4304.	6.4	48
280	In vivo skeletal imaging of 18F-fluoride with positron emission tomography reveals damage- and time-dependent responses to fatigue loading in the rat ulna. Bone, 2006, 39, 229-236.	2.9	46
281	Three-dimensional maximum a posteriori (MAP) imaging with radiopharmaceuticals labeled with three Cu radionuclides. Nuclear Medicine and Biology, 2006, 33, 217-226.	0.6	35
282	64Cu-azabicyclo[3.2.2]nonane thiosemicarbazone complexes: radiopharmaceuticals for PET of topoisomerase II expression in tumors. Journal of Nuclear Medicine, 2006, 47, 2034-41.	5.0	22
283	Radiolabeled Antibodies for Tumor Imaging and Therapy. , 2005, , 685-714.		1
284	Assessment of regional tumor hypoxia using 18F-fluoromisonidazole and 64Cu(II)-diacetyl-bis(N4-methylthiosemicarbazone) positron emission tomography: Comparative study featuring microPET imaging, Po2 probe measurement, autoradiography, and fluorescent microscopy in the R3327-AT and FaDu rat tumor models. International Journal of Radiation Oncology Biology Physics,	0.8	183
285	2005, 61, 1493-1502. A Tat Fusion Protein–Based Tumor Vaccine for Breast Cancer. Annals of Surgical Oncology, 2005, 12, 517-525.	1.5	27
286	Dosimetry of 60/61/62/64Cu-ATSM: a hypoxia imaging agent for PET. European Journal of Nuclear Medicine and Molecular Imaging, 2005, 32, 764-770.	6.4	74
287	Positron-Emitting Isotopes Produced on Biomedical Cyclotrons. Current Medicinal Chemistry, 2005, 12, 807-818.	2.4	65
288	Identification of a Novel Prostate Tumor Target, Mindin/RG-1, for Antibody-Based Radiotherapy of Prostate Cancer. Cancer Research, 2005, 65, 8397-8405.	0.9	44

#	Article	IF	CITATIONS
289	Imaging of Melanoma Using64Cuâ^' and86Yâ^'DOTAâ^'ReCCMSH(Arg11), a Cyclized Peptide Analogue of α-MSH. Journal of Medicinal Chemistry, 2005, 48, 2985-2992.	6.4	124
290	Basic characterization of 64Cu-ATSM as a radiotherapy agent. Nuclear Medicine and Biology, 2005, 32, 21-28.	0.6	93
291	Investigation into 64Cu-labeled Bis(selenosemicarbazone) and Bis(thiosemicarbazone) complexes as hypoxia imaging agents. Nuclear Medicine and Biology, 2005, 32, 147-156.	0.6	68
292	Cell line-dependent differences in uptake and retention of the hypoxia-selective nuclear imaging agent Cu-ATSM. Nuclear Medicine and Biology, 2005, 32, 623-630.	0.6	98
293	Preparation of high specific activity 86Y using a small biomedical cyclotron. Nuclear Medicine and Biology, 2005, 32, 891-897.	0.6	81
294	Measurement of input functions in rodents: challenges and solutions. Nuclear Medicine and Biology, 2005, 32, 679-685.	0.6	107
295	In vivo assessment of tumor hypoxia in lung cancer with 60Cu-ATSM. European Journal of Nuclear Medicine and Molecular Imaging, 2003, 30, 844-850.	6.4	358
296	Assessing tumor hypoxia in cervical cancer by positron emission tomography with 60Cu-ATSM: Relationship to therapeutic response—a preliminary report. International Journal of Radiation Oncology Biology Physics, 2003, 55, 1233-1238.	0.8	324
297	Polyclonal antibodies to xenogeneic endothelial cells induce apoptosis and block support of tumor growth in mice. Vaccine, 2003, 21, 2667-2677.	3.8	13
298	Intra-tumoral distribution of 64Cu-ATSM: a comparison study with FDG. Nuclear Medicine and Biology, 2003, 30, 529-534.	0.6	55
299	Preparation of 66Ga- and 68Ga-labeled Ga(III)-deferoxamine-folate as potential folate-receptor-targeted PET radiopharmaceuticals. Nuclear Medicine and Biology, 2003, 30, 725-731.	0.6	113
300	Enhancing targeted radiotherapy by copper(II)diacetyl- bis(N4-methylthiosemicarbazone) using 2-deoxy-D-glucose. Cancer Research, 2003, 63, 5496-504.	0.9	46
301	DOTAâ	3.6	69
302	Small animal imaging. European Journal of Cancer, 2002, 38, 2173-2188.	2.8	168
303	Molecular imaging: The application of small animal positron emission tomography. Journal of Cellular Biochemistry, 2002, 87, 110-115.	2.6	33
304	Copper bis(thiosemicarbazone) complexes as hypoxia imaging agents: structure-activity relationships. Journal of Biological Inorganic Chemistry, 2002, 7, 249-259.	2.6	248
305	Copper-64-pyruvaldehyde-bis(N(4)-methylthiosemicarbazone) for the prevention of tumor growth at wound sites following laparoscopic surgery: monitoring therapy response with microPET and magnetic resonance imaging. Cancer Research, 2002, 62, 445-9.	0.9	26
306	Delineation of hypoxia in canine myocardium using PET and copper(II)-diacetyl-bis(N(4)-methylthiosemicarbazone). Journal of Nuclear Medicine, 2002, 43, 1557-69.	5.0	69

#	Article	IF	CITATIONS
307	Retention mechanism of hypoxia selective nuclear imaging/radiotherapeutic agent Cu-diacetyl-bis(N) Tj ETQq1 1 0	.784314 r 2.2	gBT /Over 126
308	A novel approach to overcome hypoxic tumor resistance: Cu-ATSM-guided intensity-modulated radiation therapy. International Journal of Radiation Oncology Biology Physics, 2001, 49, 1171-1182.	0.8	410
309	Toxicity and dosimetry of177Lu-DOTA-Y3-octreotate in a rat model. International Journal of Cancer, 2001, 94, 873-877.	5.1	51
310	⁶⁴ Cuâ€₱TSM as an inhibitor of tumor recurrence. Journal of Labelled Compounds and Radiopharmaceuticals, 2001, 44, S87.	1.0	0
311	Copperâ€64/61 and iodineâ€125â€labeled dotaâ€DTYR ¹ â€octreotate: A new somatostatin analog fo labeling with metals and halogens. Journal of Labelled Compounds and Radiopharmaceuticals, 2001, 44, S948.	or 1.0	3
312	Copper-64-diacetyl-bis(N4-methylthiosemicarbazone): An agent for radiotherapy. Proceedings of the National Academy of Sciences of the United States of America, 2001, 98, 1206-1211.	7.1	192
313	64Cu-TETA-octreotide as a PET imaging agent for patients with neuroendocrine tumors. Journal of Nuclear Medicine, 2001, 42, 213-21.	5.0	203
314	Tumor uptake of copper-diacetyl-bis(N(4)-methylthiosemicarbazone): effect of changes in tissue oxygenation. Journal of Nuclear Medicine, 2001, 42, 655-61.	5.0	133
315	PET imaging of hypoxia. The Quarterly Journal of Nuclear Medicine: Official Publication of the Italian Association of Nuclear Medicine (AIMN) [and] the International Association of Radiopharmacology (IAR), 2001, 45, 183-8.	0.5	17
316	Copper bis(diphosphine) complexes: radiopharmaceuticals for the detection of multi-drug resistance in tumours by PET. European Journal of Nuclear Medicine and Molecular Imaging, 2000, 27, 638-646.	6.4	40
317	Comparative Dosimetry of Copper-64 and Yttrium-90-Labeled Somatostatin Analogs in a Tumor-Bearing Rat Model. Cancer Biotherapy and Radiopharmaceuticals, 2000, 15, 593-604.	1.0	24
318	Radiopharmaceuticals for targeted radiotherapy of cancer. Expert Opinion on Therapeutic Patents, 2000, 10, 1057-1069.	5.0	18
319	Metal complexes as diagnostic tools. Coordination Chemistry Reviews, 1999, 184, 3-66.	18.8	246
320	Utilization of metabolic, transport and receptor-mediated processes to deliver agents for cancer diagnosis. Advanced Drug Delivery Reviews, 1999, 37, 189-211.	13.7	20
321	In vitro and in vivo evaluation of 64Cu-TETA-Tyr3-octreotate. a new somatostatin analog with improved target tissue uptake. Nuclear Medicine and Biology, 1999, 26, 267-273.	0.6	88
322	High purity production and potential applications of copper-60 and copper-61. Nuclear Medicine and Biology, 1999, 26, 351-358.	0.6	140
323	Comparison of Four64Cu-Labeled Somatostatin Analogues in Vitro and in a Tumor-Bearing Rat Model:Â Evaluation of New Derivatives for Positron Emission Tomography Imaging and Targeted Radiotherapy‖. Journal of Medicinal Chemistry, 1999, 42, 1341-1347.	6.4	99
324	Evaluation of 64Cu-ATSM in vitro and in vivo in a hypoxic tumor model. Journal of Nuclear Medicine, 1999, 40, 177-83.	5.0	236

#	Article	IF	CITATIONS
325	Radiotherapy and dosimetry of 64Cu-TETA-Tyr3-octreotate in a somatostatin receptor-positive, tumor-bearing rat model. Clinical Cancer Research, 1999, 5, 3608-16.	7.0	71
326	Design of hypoxia-targeting radiopharmaceuticals: selective uptake of copper-64 complexes in hypoxic cells in vitro. European Journal of Nuclear Medicine and Molecular Imaging, 1998, 25, 788-792.	6.4	94
327	Effect of ligand and solvent on chloride ion coordination in anti-tumour copper(I) diphosphine complexes: Synthesis of [Cu(dppe)2]Cl and analogous complexes (dppe =) Tj ETQq1 1 0.784314 rgBT /Overlock 1	102.72f 50 6	5 ⊉ ∄d (1,2-bi
328	Radiotherapy, toxicity and dosimetry of copper-64-TETA-octreotide in tumor-bearing rats. Journal of Nuclear Medicine, 1998, 39, 1944-51.	5.0	85
329	Diphosphine bifunctional chelators for low-valent metal ions. Crystal structures of the copper(I) complexes [CuClL12] and [CuL12][PF6] [L1â€=â€2,3-bis(diphenylphosphino)maleic anhydride]. Journal of the Chemical Society Dalton Transactions, 1997, , 855-862.	2 1.1	20
330	Copper radionuclides and radiopharmaceuticals in nuclear medicine. Nuclear Medicine and Biology, 1996, 23, 957-980.	0.6	361
331	Copper(I) bis(diphosphine) complexes as a basis for radiopharmaceuticals for positron emission tomography and targeted radiotherapy. Chemical Communications, 1996, , 1093.	4.1	30
332	Rhenium complex of a triply deprotonated chelated thiosemicarbazide and its conversion to a nitride complex via a hydrazide intermediate. Crystal structure of [ReCl2(NH)(NHNH2)(PPh3)2]. Journal of the Chemical Society Dalton Transactions, 1995, , 1357.	1.1	19
333	The preparation of rhenium(V) oxo and imido complexes with Et2NCSNHCOPh and Et2NCSBC(NH)Ph. The x-ray crystal structure of [ReOCl(PhCONCSNEt2)2]. Polyhedron, 1993, 12, 221-225.	2.2	15